

Error mitigation with Clifford quantum-circuit data

Piotr Czarnik, Andrew Arrasmith, Patrick J. Coles, and Lukasz Cincio
Theoretical Division, Los Alamos National Laboratory, Los Alamos, NM 87545, USA.

Achieving near-term quantum advantage will require accurate estimation of quantum observables despite significant hardware noise. For this purpose, we propose a novel, scalable error-mitigation method that applies to gate-based quantum computers. The method generates training data $\{X_i^{\text{noisy}}, X_i^{\text{exact}}\}$ via quantum circuits composed largely of Clifford gates, which can be efficiently simulated classically, where X_i^{noisy} and X_i^{exact} are noisy and noiseless observables respectively. Fitting a linear ansatz to this data then allows for the prediction of noise-free observables for arbitrary circuits. We analyze the performance of our method versus the number of qubits, circuit depth, and number of non-Clifford gates. We obtain an order-of-magnitude error reduction for a ground-state energy problem on a 16-qubit IBMQ quantum computer and on a 64-qubit noisy simulator.

Introduction.—Currently, one of the great unsolved technological questions is whether near-term quantum computers will be useful for practical applications. These noisy intermediate-scale quantum (NISQ) devices do not have enough qubits or high enough gate fidelities for fault-tolerant quantum error correction [1]. Consequently, any observable measured on a NISQ device will have limited accuracy. However, candidate applications such as quantum chemistry require chemical accuracy to beat classical methods [2, 3]. Similarly quantum approximate optimization has the potential to beat classical optimization when high accuracy is achieved [4–6].

Hence, it is widely regarded that near-term quantum advantage will only be achieved through error mitigation. Error mitigation (EM) is broadly defined as methods that reduce the impact of noise, rather than directly correct it. EM includes efforts to optimize quantum circuits with compiling and machine learning [7, 8]. It also includes variational quantum algorithms [9–11], some of which can be used to remove the effects of incoherent noise [12–16]. A prominent EM approach is to perform classical post-processing of observable expectation values. This includes the most widely used, state-of-the-art example known as zero-noise extrapolation (ZNE), which has shown great promise [17, 18].

ZNE involves collecting data at various levels of noise, achieved by stretching gate times, and using this noisy data to extrapolate an observable’s expectation value to the zero-noise limit [19, 20]. It has been successfully employed to correct ground-state energies for problem sizes up to 4-qubits [17, 18, 21]. In principle the method is scalable since it only adds overhead that is linear in the number of gates. However, ZNE only corrects noise up to a certain expansion order and hence it relies on the assumption of low noise levels, an assumption that could be challenged for deep, large-scale circuits.

A crucial requirement of any EM method is scalability. While it is relatively easy to develop EM methods for small qubit systems, EM methods that work effectively at the quantum supremacy scale (> 50 qubits) are much more challenging to construct. Even methods that are in principle scalable may not actually scale well in practice.

This work aims to address this issue by proposing a

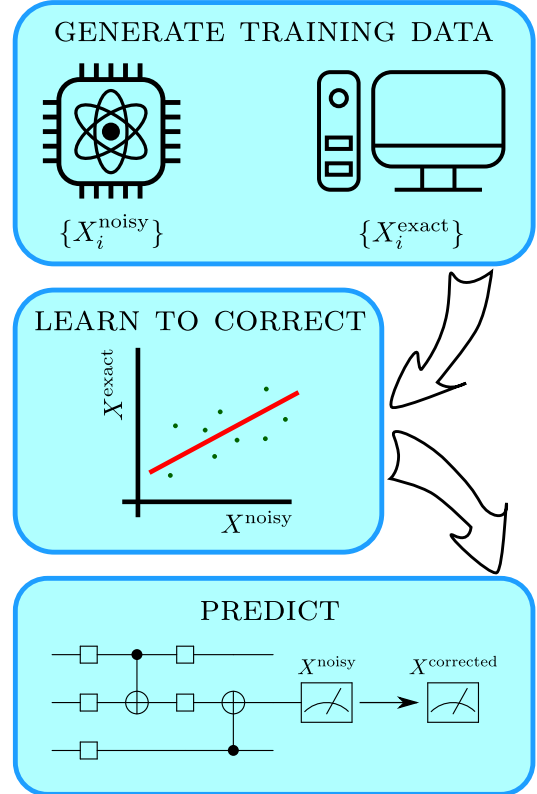


FIG. 1. Our proposed error mitigation method. For a set of states that are classically simulable, one generates noisy and corresponding noise-free data on a quantum computer and classical computer, respectively. One learns to correct on this training data by fitting the parameters of an ansatz. Finally, one uses this ansatz with the fitted parameters to predict noise-free observables for arbitrary quantum states.

novel, scalable EM method that is applicable to all gate-based quantum computers. The basic idea is shown in Fig. 1. First we generate training data, of the form $\{X_i^{\text{noisy}}, X_i^{\text{exact}}\}$, where X_i^{noisy} and X_i^{exact} are the noisy and noiseless versions of an observable’s expectation value of interest. The noisy values are obtained directly from the quantum computer, while the noiseless values are simulated on a classical computer. Scalability is

achieved by generating the training data from quantum circuits composed largely of Clifford gates (gates that map Pauli operators to Pauli operators), and hence these circuits are efficiently classically simulable. Next we fit the training data with a model, and finally we use the fitted model to predict the noise-free observable.

Our method is conceptually simple and could be refined with sophisticated model fitting methods offered by modern machine learning [22]. Nevertheless, even with simple linear-regression-based fitting, our method performs extremely well in practice. We consider the task of estimating the ground-state energy of an Ising spin chain by variationally training the Quantum Alternating Operator Ansatz (QAOA) [4, 5]. For this task, our method reduces the error by an order-of-magnitude for both a 16-qubit problem solved on IBMQ quantum computer and a 64-qubit problem solved on a noisy simulator. We also demonstrate the utility of our method for non-variational algorithms such as quantum phase estimation. Finally we find that our method appears to perform better than ZNE for larger scale problems.

Our method.—We refer to our method as Clifford Data Regression (CDR). Let X be the observable of interest whose expectation value $X_\psi^{\text{exact}} = \langle \psi | X | \psi \rangle$ one wishes to estimate for a given state $|\psi\rangle$. Let X_ψ^{noisy} be the noisy version of this expectation value obtained from the quantum computer. To remove the noise from this expectation value, the CDR method involves the following steps:

1. One chooses a set of states $\mathcal{S}_\psi = \{|\phi_i\rangle\}$ that will be used to construct the training data \mathcal{T}_ψ . Each $|\phi_i\rangle$ state must satisfy the property that it is efficient to classically compute the expectation value of X for this state. The CDR method ensures this property by constructing each $|\phi_i\rangle$ state from a quantum circuit composed largely of Clifford gates. We denote the number of non-Clifford gates used to prepare each $|\phi_i\rangle$ as N , which (as shown below) plays the role of a refinement parameter.
2. For each $|\phi_i\rangle \in \mathcal{S}_\psi$, one evaluates $X_{\phi_i}^{\text{exact}} = \langle \phi_i | X | \phi_i \rangle$ using a classical computer. One also evaluates the noisy version of this expectation value, $X_{\phi_i}^{\text{noisy}}$, using the quantum computer of interest. These two quantities are incorporated into the training data set $\mathcal{T}_\psi = \{X_{\phi_i}^{\text{noisy}}, X_{\phi_i}^{\text{exact}}\}$.
3. One constructs an ansatz or model for the noise-free value of the observable in the vicinity of $|\psi\rangle$,

$$X_\psi^{\text{exact}} = f(X_\psi^{\text{noisy}}, \mathbf{a}), \quad (1)$$

where \mathbf{a} are free parameters. The parameters can be found either by regression or machine-learning methods. In this article we use least square regression, with a linear ansatz:

$$f(X_\psi^{\text{noisy}}, \mathbf{a}) = a_1 X_\psi^{\text{noisy}} + a_2, \quad (2)$$

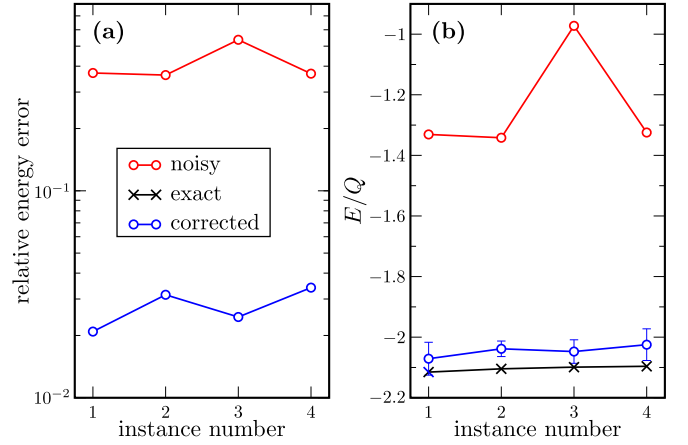


FIG. 2. Correcting the ground-state energy of the 16-qubit Ising model with our CDR method. The ground states were prepared by optimizing a $p = 2$ QAOA circuit on IBM’s Almaden quantum processor. (a) The relative energy error is plotted for the noisy (red) and corrected (blue) results for several optimization instances. (b) The inferred energy per qubit, E/Q , is plotted, along with the exact values (black). The error bars are explained in the text.

obtaining parameters a_1 and a_2 by minimizing

$$C = \sum_{\phi_i \in \mathcal{S}_\psi} (X_{\phi_i}^{\text{exact}} - (a_1 X_{\phi_i}^{\text{noisy}} + a_2))^2. \quad (3)$$

4. One uses the ansatz $f(X_\psi^{\text{noisy}}, \mathbf{a})$ with the fitted parameters to correct X_ψ^{noisy} .

We now discuss several strategies for how to choose \mathcal{S}_ψ in Step 1. In general, we have found that it is advantageous to tailor the set \mathcal{S}_ψ to the specific state $|\psi\rangle$; in other words, to bias the training data towards the target state of interest. A simple strategy for this purpose is to generate the state-preparation circuits for the $|\phi_i\rangle$ states by replacing a subset of the gates in the circuit that prepares $|\psi\rangle$ with Clifford gates that are close in distance to the original gates. An alternative strategy, which is used in our implementations, is to employ Markov Chain Monte Carlo (MCMC) to generate classically-simulable states $|\phi_i\rangle$ based on the values of their observables. (See Appendix A for further details.)

In general, one may base the MCMC sampling on the closeness of $X_{\phi_i}^{\text{noisy}}$ to X_ψ^{noisy} . However, a potentially more efficient strategy exists for the specific application of variational quantum algorithms [9–11]. When $|\psi\rangle$ is a state that is meant to optimize a variational cost function (e.g., the energy of a given Hamiltonian), then one can instead base the sampling on minimizing this cost function. In this way, one can employ MCMC to obtain classically-simulable states that are close to extremizing the variational cost function.

Implementation for QAOA.—A central application of error mitigation is to correct the energies of Hamiltonian

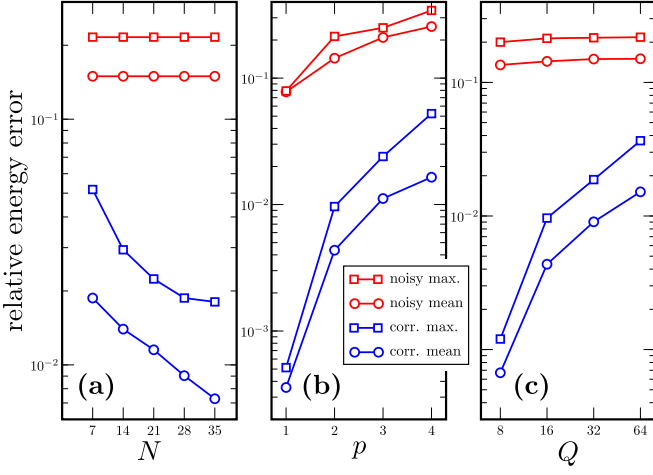


FIG. 3. Correcting the ground-state energy of the Ising model with our CDR method. The ground states were prepared by optimizing a QAOA circuit on a noisy simulator. The mean (circles) and maximal (squares) relative energy error is plotted for the noisy (red) and corrected (blue) results. (a) The results for $Q = 32, p = 2$ plotted versus N . (b) The results for $Q = 16, N = 28$ plotted versus p . (c) The results for $p = 2, N = 28$ plotted versus Q .

eigenstates prepared on a quantum computer. Here we illustrate this application with the Quantum Alternating Operator Ansatz (QAOA) [4, 5], which can serve as an ansatz for Hamiltonian ground states. We consider the transverse Ising model, given by

$$H = -g \sum_j \sigma_X^j - \sum_{\langle j, j' \rangle} \sigma_Z^j \sigma_Z^{j'}, \quad (4)$$

where σ_X, σ_Z are Pauli operators and $\langle j, j' \rangle$ denotes a sum over nearest neighbors. We study the case of $g = 2$ (belonging to a paramagnetic phase) with open boundary conditions for different numbers of qubits Q . To apply the QAOA, we write $H = H_1 + H_2$ with $H_2 = -g \sum_j \sigma_X^j$ and $H_1 = -\sum_{\langle j, j' \rangle} \sigma_Z^j \sigma_Z^{j'}$. Then the QAOA is

$$\prod_{j=p, p-1, \dots, 1} e^{i\beta_j H_2} e^{i\gamma_j H_1} (|+\rangle)^{\otimes Q}, \quad (5)$$

where β_j, γ_j are variational parameters, p is the number of ansatz layers, and $|+\rangle = (|0\rangle + |1\rangle)/\sqrt{2}$. The exponentials of H_2 and H_1 can be easily decomposed into quantum circuits (see Appendix C).

For this implementation, we first perform the optimization of the β_j, γ_j parameters, and then we correct the energies of low-energy local minima of this optimization. This correction involves correcting all $\langle \sigma_X^j \rangle$ and $\langle \sigma_Z^j \sigma_Z^{j'} \rangle$ terms associated with (4). (Note however that the same training set \mathcal{S}_ψ , which is generated based on the total energy, is used to correct each term.) Figure 2 shows that our CDR method reduces the relative energy error by an order-of-magnitude on IBM's Almaden quantum processor [23]. We show error bars that reflect our confidence

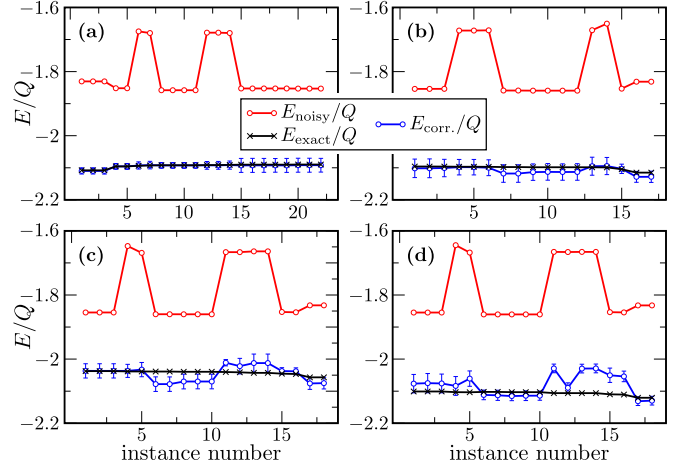


FIG. 4. Inferred energy per qubit, E/Q , for minima obtained from various optimization instances of the QAOA circuit for the Ising model on a noisy simulator. The noisy, exact, and corrected results correspond to the red, blue, and black curves, respectively. The results were obtained with $p = 2$ and $N = 28$ for various qubit numbers: (a) $Q = 8$, (b) $Q = 16$, (c) $Q = 32$, and (d) $Q = 64$. The relative errors for these minima were analyzed in Fig. 3(c). The error bars are explained in the text.

in our ability to correct the training data. Specifically we take the error bars as three standard deviations, where the standard deviation is obtained directly from the cost function in (3) by dividing C by the training size and then taking the square root (see Appendix B).

To study the scaling behavior, we also implement this problem using a classical matrix-product-state [24] simulator that incorporates a noise model obtained from gate set tomography of IBM's Ourense quantum computer. Figure 3 presents the relative energy error, uncorrected (red) and corrected (blue), for different values of N , p , and Q . One can see that our CDR method results in between one to two orders-of-magnitude reduction in the error. Increasing the number of non-Clifford gates N in the training data monotonically reduces the error, as shown in Fig. 3(a). This is expected because increasing N allows the training set \mathcal{S}_ψ to become closer to the target state $|\psi\rangle$ of interest. Hence, our results show that N is a refinement parameter, allowing one to obtain better error mitigation with the increased computational difficulty of simulating more non-Clifford gates. N is limited to $\lesssim 50$ for state-of-the-art classical simulators, but our results show that $N \lesssim 30$ already leads to orders-of-magnitude reduction in the error.

Figures 3(b) and (c) show that correcting errors with CDR becomes more challenging with deeper circuits and larger qubit counts, respectively. However, the rate of error growth with p and Q is not very sharp, and we still obtain large error reductions for either $p = 4$ layers or 64 qubits. It is worth noting that 64 qubits is considered to be in the regime where quantum supremacy might be demonstrated [25].

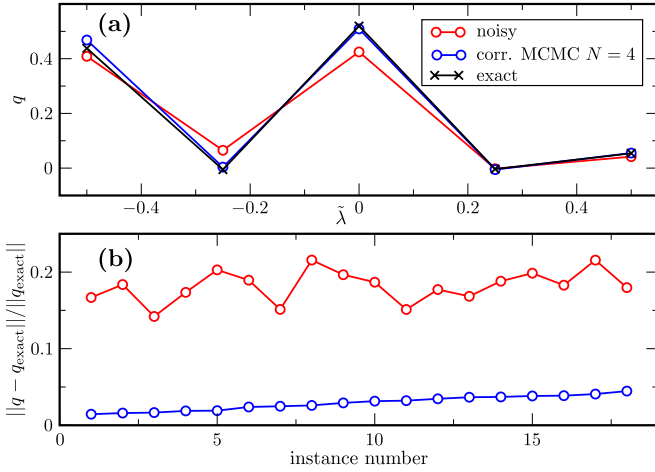


FIG. 5. Correcting the results of quantum phase estimation on a noisy simulator with CDR. (a) Decomposition of a random pure state in the binned eigenbasis of \tilde{H} defined in the text, without (red) and with (blue) correction. The probability distribution q is shown as a function of the binned energy eigenvalue $\tilde{\lambda}$. The random state whose decomposition is shown is the one for which CDR performed most poorly. (b) Relative error of this decomposition over 18 instances (different random pure states), ordered by increasing corrected error. For all of these instances, we employ training data constructed from quantum circuits with 4 of the total 8 non-Clifford gates replaced by Clifford gates (see Appendix D).

To give further insight into the scaling with Q , we show the results for individual optimization instances in Fig. 4. Interestingly, Fig. 4 shows that the CDR method is capable of removing noise-induced fluctuations in the energy, i.e., very different noisy energy values are correctly mapped to the same corrected ground-state energy values. For large Q , some remnant of these fluctuations still linger in the corrected energies, leading to the worse performance in Fig. 3(c), although it suggests that employing a more detailed model in (1) accounting for additional features in the training data could further improve the accuracy of the corrected ground state energy.

Remark on applying ZNE.—In addition to applying our CDR method for QAOA, we also examined the performance of the ZNE method under the same conditions as those in Fig. 2, i.e., for the $Q = 16$, $p = 2$ case with the same circuits on IBM’s Almaden quantum processor. Unfortunately, for this problem instance we were unable to attain a meaningful correction with ZNE. This difficulty was likely largely due to the size and depth of the quantum circuit we considered, as ZNE depends on the base circuit being considered not being too noisy to start with. For more details, see Appendix E.

Implementation for phase estimation.—Let us now illustrate how our method applies to quantum phase estimation. We consider a near-term version of phase estimation that only requires a single ancilla [26]. For an input

state $|\chi\rangle$, this algorithm estimates $\langle\chi|e^{-iHt}|\chi\rangle = \langle e^{-iHt}\rangle$ on a quantum computer for a series of times t and then classically Fourier transforms the time series to estimate eigenvalues of H . The expectation value $\langle e^{-iHt}\rangle$ is obtained by measuring $\langle\sigma_X + i\sigma_Y\rangle$ on an ancilla qubit after applying the controlled e^{-iHt} gate to the state $|\chi\rangle$ [26].

We performed error mitigation of $\langle e^{-i\tilde{H}t}\rangle = \langle\sigma_X + i\sigma_Y\rangle$ for a two-qubit Hamiltonian $\tilde{H} = -g\sum_{j=1}^Q\sigma_X^j$, with $g = 1/(2Q)$, $|\chi\rangle$ being a random pure state, and times $t \in \{1, 2, \dots, 40\}$. See Appendix D for quantum circuits used in the computation. We employed the same noisy simulator as that used for the QAOA implementation in Figs. 3-4. The results are shown in Fig. 5. One can see in Fig. 5(a) that the decomposition of $|\chi\rangle$ in the energy eigenbasis is significantly improved after correction with the CDR method. Indeed, Fig. 5(b) shows that the relative error is reduced by at least a factor of four by CDR.

Conclusions.—With quantum supremacy recently demonstrated [25], the next milestone in quantum computing may be to achieve quantum advantage for practical applications such as chemistry or optimization. These applications will require accurate estimation of observables on noisy quantum hardware, and hence large-scale error mitigation will be necessary. In this work, we proposed a scalable method to significantly reduce the errors (potentially by orders of magnitude) of quantum observables. The method, called Clifford Data Regression (CDR), learns how to correct errors on a training data set. Constructing this training set exploits the classical simulability of quantum circuits composed largely of Clifford gates. This allows our method to scale to large problem size, and indeed we obtained meaningful corrections with CDR for a 64-qubit ground-state-energy problem.

Further testing our method on real quantum hardware will be important. In addition, refining our method with ansatzes that are more sophisticated than our linear ansatz (e.g., using neural networks or other machine-learning approaches) could be fruitful. Finally, it would be interesting to extend the applicability of our approach to analog quantum simulators.

Acknowledgements.—We thank Kipton Barros, Kenneth Rudinger, and Mohan Sarovar for helpful conversations. We thank IBM for providing access to their quantum computers. The views expressed in this article are those of the authors and do not reflect those of IBM. All authors acknowledge support from LANL’s Laboratory Directed Research and Development (LDRD) program. PJC also acknowledges support from the LANL ASC Beyond Moore’s Law project. This work was also supported by the U.S. Department of Energy (DOE), Office of Science, Office of Advanced Scientific Computing Research, under the Quantum Computing Application Teams program.

Note Added.—After completion of this work, we noticed related work was very recently posted [27].

-
- [1] John Preskill, “Quantum computing in the NISQ era and beyond,” *Quantum* **2**, 79 (2018).
- [2] Yudong Cao, Jonathan Romero, Jonathan P Olson, Matthias Degroote, Peter D Johnson, Mária Kieferová, Ian D Kivlichan, Tim Menke, Borja Peropadre, Nicolas PD Sawaya, *et al.*, “Quantum chemistry in the age of quantum computing,” *Chemical reviews* **119**, 10856–10915 (2019).
- [3] Sam McArdle, Suguru Endo, Alan Aspuru-Guzik, Simon C Benjamin, and Xiao Yuan, “Quantum computational chemistry,” *Reviews of Modern Physics* **92**, 015003 (2020).
- [4] E. Farhi, J. Goldstone, and S. Gutmann, “A quantum approximate optimization algorithm,” *arXiv:1411.4028 [quant-ph]*.
- [5] Stuart Hadfield, Zhihui Wang, Bryan O’Gorman, Eleanor G Rieffel, Davide Venturelli, and Rupak Biswas, “From the quantum approximate optimization algorithm to a quantum alternating operator ansatz,” *Algorithms* **12**, 34 (2019).
- [6] G. E. Crooks, “Performance of the quantum approximate optimization algorithm on the maximum cut problem,” *arXiv:1811.08419 [quant-ph]*.
- [7] L. Cincio, Y. Subaşı, A. T. Sornborger, and P. J. Coles, “Learning the quantum algorithm for state overlap,” *New Journal of Physics* **20**, 113022 (2018).
- [8] Prakash Murali, Jonathan M Baker, Ali Javadi-Abhari, Frederic T Chong, and Margaret Martonosi, “Noise-adaptive compiler mappings for noisy intermediate-scale quantum computers,” in *Proceedings of the Twenty-Fourth International Conference on Architectural Support for Programming Languages and Operating Systems* (2019) pp. 1015–1029.
- [9] A. Peruzzo, J. McClean, P. Shadbolt, M.-H. Yung, X.-Q. Zhou, P. J. Love, A. Aspuru-Guzik, and J. L. O’Brien, “A variational eigenvalue solver on a photonic quantum processor,” *Nature Communications* **5**, 4213 (2014).
- [10] Jarrod R McClean, Jonathan Romero, Ryan Babbush, and Alán Aspuru-Guzik, “The theory of variational hybrid quantum-classical algorithms,” *New Journal of Physics* **18**, 023023 (2016).
- [11] Xiao Yuan, Suguru Endo, Qi Zhao, Ying Li, and Simon C Benjamin, “Theory of variational quantum simulation,” *Quantum* **3**, 191 (2019).
- [12] Y. Li and S. C. Benjamin, “Efficient variational quantum simulator incorporating active error minimization,” *Phys. Rev. X* **7**, 021050 (2017).
- [13] S. Khatri, R. LaRose, A. Poremba, L. Cincio, A. T. Sornborger, and P. J. Coles, “Quantum-assisted quantum compiling,” *Quantum* **3**, 140 (2019).
- [14] Kunal Sharma, Sumeet Khatri, Marco Cerezo, and Patrick J Coles, “Noise resilience of variational quantum compiling,” *New Journal of Physics* **22**, 043006 (2020).
- [15] Ryan LaRose, Arkin Tikku, Étude O’Neel-Judy, Lukasz Cincio, and Patrick J Coles, “Variational quantum state diagonalization,” *npj Quantum Information* **5**, 1–10 (2019).
- [16] M Cerezo, Kunal Sharma, Andrew Arrasmith, and Patrick J Coles, “Variational quantum state eigensolver,” *arXiv preprint arXiv:2004.01372* (2020).
- [17] Abhinav Kandala, Kristan Temme, Antonio D Córcoles, Antonio Mezzacapo, Jerry M Chow, and Jay M Gambetta, “Error mitigation extends the computational reach of a noisy quantum processor,” *Nature* **567**, 491–495 (2019).
- [18] Eugene F Dumitrescu, Alex J McCaskey, Gaute Hagen, Gustav R Jansen, Titus D Morris, T Papenbrock, Raphael C Pooser, David Jarvis Dean, and Pavel Lougovski, “Cloud quantum computing of an atomic nucleus,” *Physical review letters* **120**, 210501 (2018).
- [19] Kristan Temme, Sergey Bravyi, and Jay M Gambetta, “Error mitigation for short-depth quantum circuits,” *Physical review letters* **119**, 180509 (2017).
- [20] Matthew Otten and Stephen K Gray, “Recovering noise-free quantum observables,” *Physical Review A* **99**, 012338 (2019).
- [21] Andre He, Benjamin Nachman, Wibe A de Jong, and Christian W Bauer, “Resource efficient zero noise extrapolation with identity insertions,” *arXiv preprint arXiv:2003.04941* (2020).
- [22] Michael A Nielsen, *Neural networks and deep learning*, Vol. 2018 (Determination press San Francisco, CA, USA:, 2015).
- [23] “IBM Q: Quantum devices and simulators,” <https://www.research.ibm.com/ibm-q/technology/devices/>, [Online; accessed May 18, 2020].
- [24] M. Fannes, B. Nachtergaele, and R. F. Werner, “Finitely correlated states on quantum spin chains,” *Communications in Mathematical Physics* **144**, 443–490 (1992).
- [25] Frank Arute, Kunal Arya, Ryan Babbush, Dave Bacon, Joseph C Bardin, Rami Barends, Rupak Biswas, Sergio Boixo, Fernando GSL Brandao, David A Buell, *et al.*, “Quantum supremacy using a programmable superconducting processor,” *Nature* **574**, 505–510 (2019).
- [26] Rolando D Somma, “Quantum eigenvalue estimation via time series analysis,” *New Journal of Physics* **21**, 123025 (2019).
- [27] Armands Strikis, Dayue Qin, Yanzhu Chen, Simon C. Benjamin, and Ying Li, “Learning-based quantum error mitigation,” *arXiv preprint arXiv:2005.07601* (2020).
- [28] Don Van Ravenzwaaij, Pete Cassey, and Scott D Brown, “A simple introduction to markov chain monte-carlo sampling,” *Psychonomic bulletin & review* **25**, 143–154 (2018).
- [29] Abhijith J., Adetokunbo Adedoyin, John Ambrosiano, Petr Anisimov, Andreas Bärtzsch, William Casper, Gopinath Chennupati, Carleton Coffrin, Hristo Djidjev, David Gunter, Satish Karra, Nathan Lemons, Shizeng Lin, Alexander Malyzhenkov, David Mascarenas, Susan Mniszewski, Balu Nadiga, Daniel O’Malley, Diane Oyen, Scott Pakin, Lakshman Prasad, Randy Roberts, Phillip Romero, Nandakishore Santhi, Nikolai Sinitsyn, Pieter J. Swart, James G. Wendelberger, Boram Yoon, Richard Zamora, Wei Zhu, Stephan Eidenbenz, Patrick J. Coles, Marc Vuffray, and Andrey Y. Lokhov, “Quantum algorithm implementations for beginners,” (2018), *arXiv:1804.03719 [cs.ET]*.
- [30] Héctor Abraham *et al.*, “Qiskit: An open-source framework for quantum computing,” (2019).

Supplemental Material for “Error mitigation with Clifford quantum-circuit data”

Here we provide additional details regarding the methods and implementations discussed in the main body of the paper.

Appendix A: Generating the set \mathcal{S}_ψ

We use a Markov Chain Monte Carlo (MCMC) [28] sampling technique in order to generate a set of classically simulable training states, \mathcal{S}_ψ , for use in CDR. Starting from some initial simulable circuit, we build \mathcal{S}_ψ by making small update steps to our circuit. At each update step, we choose to either accept or reject the change. On accepting a new circuit it is added to \mathcal{S}_ψ , and we look for updates starting from this new circuit. This process is repeated until we have generated as many circuits as desired for \mathcal{S}_ψ .

In our applications, the initial point is chosen by finding a near-Clifford circuit with N non-Clifford gates that is close to the circuit we wish to correct. To generate update steps, we randomly pick n_p pairs of the circuit’s σ_Z rotations. Here, each pair consists of one rotation that has been replaced by a Clifford gate (specifically, S^n for some integer n where $S = R_Z(\pi/4) = e^{-i\sigma_Z\pi/8}$ is the $\pi/4$ rotation gate) and one that has not. We chose $n_p = 5$ in our implementations. For each pair we then replace the non-Clifford rotation by a power of S and the Clifford gate by the original rotation in that part of the circuit. When replacing a rotation $R_Z(\alpha)$ by S^n , the power n is randomly sampled with weight $w(n)$, which is given by

$$w(n) = e^{-d^2/\sigma^2}, \quad d = ||R_Z(\alpha) - S^n||, \quad (\text{A1})$$

with $\sigma = 1/2$. Note that such an update preserves the number of non-Clifford gates N .

For our implementations, the new state $|\phi\rangle$ proposed by this update step is then either accepted or rejected according to a Metropolis-Hastings rule with a likelihood function L . This likelihood was defined differently for our QAOA and phase estimation examples. For QAOA we used

$$L(X_\phi^{\text{exact}}) \propto e^{-(X^{\text{exact}} - X_0)^2/X_\sigma^2}. \quad (\text{A2})$$

Here, X is the energy per qubit, and $X_0 = -2.1$ being roughly X_ψ^{exact} . We used $X_\sigma = 0.05$, though we found that instead using $X_\sigma = 0.1$ or 0.2 produced similar results. Larger values ($X_\sigma \sim 1$) degraded the quality of the results. We note that when correcting more general minimization problems we could have simply used a different form that assigned higher likelihoods to lower values of the observable instead.

For the phase estimation example, we used a similar expression:

$$L(X_\phi^{\text{noisy}}) \propto e^{-(X_\phi^{\text{noisy}} - X_\psi^{\text{noisy}})^2/X_\sigma^2}, \quad (\text{A3})$$

with $X_\sigma = 0.1$. This version is appropriate when correcting observables that we do not have special information about (e.g., that X is not supposed to be minimized).

Appendix B: Error bars

In the main text, we display error bars on the corrected observables obtained by the CDR method. These error bars are meant to convey one’s confidence in the predicted noise-free observable. Conceptually speaking, there are two main sources of error to consider: (1) Imperfect training on the training data such that the cost function C does not go to zero, and (2) Inability of the training data to capture the noise processes that affect the target state $|\psi\rangle$. The latter source of error is difficult to quantify in practice, although it can be systematically removed by increasing the number of non-Clifford gates N as discussed in the main text.

Therefore we focus our error bars on the former source of error, i.e., imperfect training. For the most part, we find (see Fig. 4) that the error bars associated with imperfect training are sufficient to encompass the discrepancy between the predicted and exact observable values. However, for our largest implementation, $Q = 64$ in Fig. 4(d), one can see that our error bars sometimes underestimate the true error. This suggests that our error bars are useful as lower bounds on the true error.

As mentioned in the main text, we calculate our error bars using the value of the cost function C obtained after training. Specifically, the magnitude of the error bar is given by three standard deviations, where the standard deviation is given by $\sqrt{C/(L-1)}$, where L is the number of states in the training set \mathcal{S}_ψ .

Appendix C: QAOA circuit structure

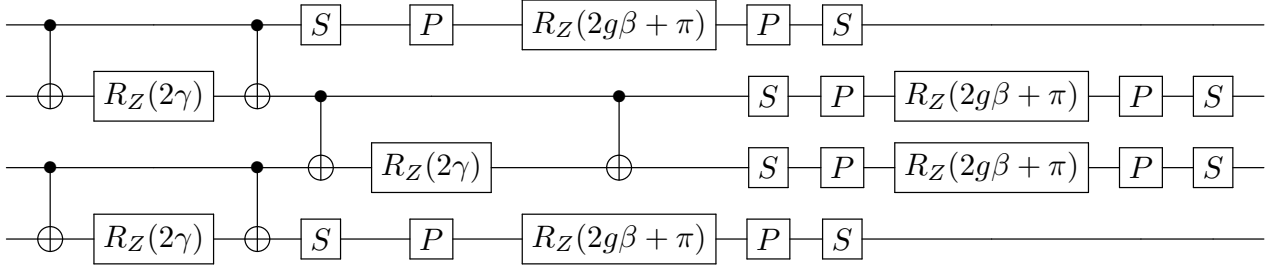


FIG. C.1. A circuit implementing a layer of the QAOA ansatz for $Q = 4$. β, γ are QAOA parameters. Here $P = R_X(\pi/2) = e^{-i\sigma_X \pi/4}$ and is a Clifford gate. The only non-Clifford gates in this circuit are the σ_Z rotations: $R_Z(\alpha) = e^{-i\sigma_Z \alpha/2}$. We note that we have made use of the decomposition of $e^{i\gamma\sigma_Z^j\sigma_Z^{j'}}$ from Ref. [29].

Figure C.1 shows the structure of our QAOA circuit for the Ising spin chain considered in the main text. We note that all gates except for the $(2(Q-1)p)$ σ_Z rotations are Clifford gates. The only changes made to this circuit for generating the training data \mathcal{S}_ψ are therefore only replacements of these σ_Z rotations by S^n , as discussed in Appendix A.

Appendix D: Quantum Phase Estimation circuit structure

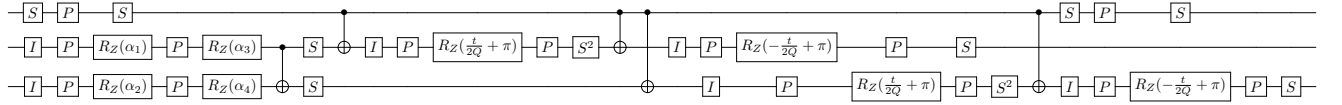


FIG. D.1. Quantum circuit used to estimate $\text{Re}(\langle \chi | e^{-i\tilde{H}t} | \chi \rangle)$ for $\tilde{H} = -g \sum_j \sigma_Z^j$, $g = 1/(2Q)$, $Q = 2$, and a random product state $|\chi\rangle$ given by random angles $\alpha_1, \alpha_2, \alpha_3, \alpha_4$.

Figure D.1 shows the quantum phase estimation circuit from Ref. [26] applied to a randomly chosen input product state. As in the QAOA ansatz, we note that all gates except for the σ_Z rotations are Clifford gates. Again, our classically simulable training data set \mathcal{S}_ψ is generated by replacing some of these σ_Z rotations with S^n as discussed in Appendix A.

Appendix E: Zero Noise Extrapolation

For comparison with our CDR method, we have performed zero noise extrapolation (ZNE) for the QAOA implementations discussed in the main text on IBM's 20-qubit Almaden quantum processor [23]. Specifically, we used Qiskit's Pulse package [30] to systematically stretch the microwave pulse sequences used to physically implement our $Q = 16$, $p = 2$ optimized QAOA circuits as done in Ref. [17].

1. Background

Following Ref. [19], the evolution of the quantum computer can be modeled in terms of the drive Hamiltonian described by the quantum circuit, $K(t)$ and a Lindblad operator $\mathcal{L}(\rho)$ representing the physical noise channels:

$$\frac{\partial}{\partial t} \rho(t) = -i[K(t), \rho(t)] + \lambda \mathcal{L}(\rho(t)). \quad (\text{E1})$$

Here λ is a (hopefully) small parameter that represents the strength of the action of the noise channels, so the limit $\lambda \rightarrow 0$ would represent noiseless quantum computation. Attempting to approximate this limit is the heart of ZNE. While an experimenter cannot in general directly adjust λ , under the assumption that the form of \mathcal{L} is invariant under time re-scaling and independent of $K(t)$, one can in effect increase λ .

Increasing λ is accomplished by increasing (stretching) the time for the circuit evolution (T) by a factor of c while decreasing the magnitude of the drive Hamiltonian:

$$\begin{aligned} T &\rightarrow T' = cT, \\ K(t) &\rightarrow K'(t) = c^{-1}K(c^{-1}t). \end{aligned} \tag{E2}$$

To see how this works, let us integrate (E1) with respect to time from $t = 0$ to $t = T'$, using our modified drive Hamiltonian from (E2). Calling the state evolved this way $\rho'(t) = \rho(c^{-1}t)$, we have:

$$\begin{aligned} \rho'(T') &= \rho(0) - i \int_0^{cT} [K'(t), \rho'(t)] dt + \lambda \int_0^{cT} \mathcal{L}(\rho'(t)) dt \\ &= \rho(0) - i \int_0^{T'} [K(t), \rho(t')] dt' + c\lambda \int_0^{T'} \mathcal{L}(\rho(t')) dt'. \end{aligned} \tag{E3}$$

We therefore have that, under these assumptions, the final state driven over a longer time with the stretched drive Hamiltonian is equivalent to one evolved with the original drive Hamiltonian with $\lambda \rightarrow c\lambda$. For a more detailed derivation of this formalism, see Ref. [19].

2. Implementation

For our implementation, we follow Ref. [17] in choosing the stretch factors $c \in \{1, 1.1, 1.25, 1.5\}$. We then stretched the pulse sequences generated from the QAOA circuit as shown in Fig. E.1. In addition to running the circuit at different stretch factors, we also made use of Qiskit's built-in measurement error mitigation functions [30] as ZNE does not directly handle read-out error. Finally, we used 212992 shots to measure each operator for each value of c .

3. Results

The data points we measured as well as our extrapolated energies are shown in Fig. E.2 for the three instances of low energy QAOA studied in the main text. For the sake of completeness, we show the extrapolation with a linear fit, a quadratic fit, and finally the cubic polynomial that is the standard ZNE approach for four values of c [17, 19]. As shown in Fig. E.2, it appears that for our particular use case the ZNE method did not provide an accurate correction for the energy expectation values.

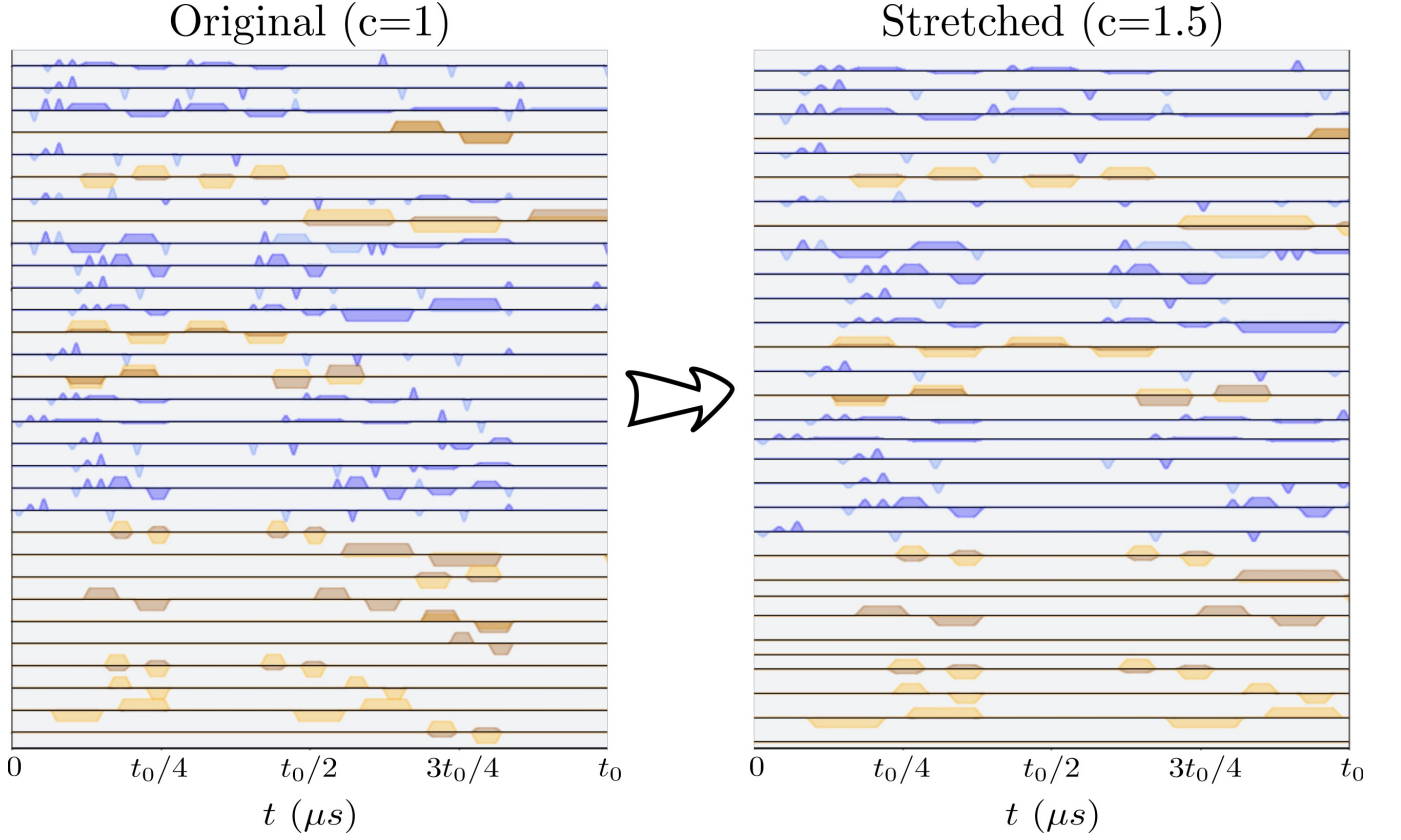


FIG. E.1. Stretching the QAOA circuit pulse sequence. The first $t_0 = 2.22 \mu s$ of the pulse sequences for a $Q = 16$, $p = 2$ QAOA circuit with $c = 1$ and $c = 1.5$ are shown. In the stretched case the pulse envelopes are lower amplitude but longer in duration. For convenience, the amplitude of the pulse envelopes shown have been normalized between the channels (shown as horizontal lines), but the normalizations are the same between the $c = 1$ and $c = 1.5$ cases.

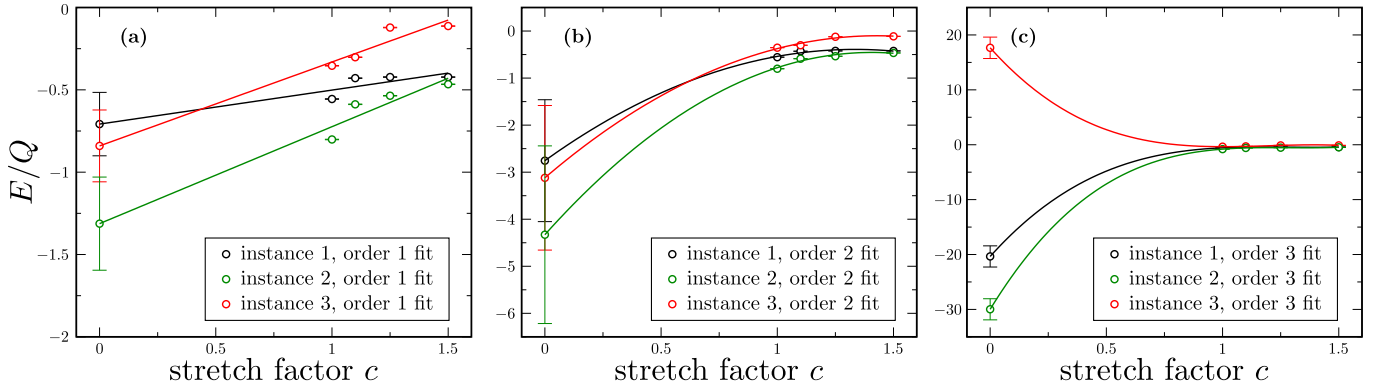


FIG. E.2. Extrapolating the stretched circuit data. Note that the error bars displayed here represent the uncertainties of the fit for $c = 0$ and the uncertainty from finite statistics for $c \in \{1, 1.1, 1.25, 1.5\}$. Note also that the third order fit is equivalent to using equation (3) in [19]. For reference, the true values of E/Q for instances 1, 2, and 3 are roughly -2.1153 , -2.1045 , and -2.0990 , respectively. These instances correspond to the first three instances shown in Fig. 2.